JPE

Load and Mutual Inductance Identification Method for Series-Parallel Compensated IPT Systems

Long Chen*, Yu-Gang Su†*, Yu-Ming Zhao*, Chun-Sen Tang* and Xin Dai*

†State Key Laboratory of Power Transmission Equipment and System Security and New Technology, Chongqing University, Chongqing, China

*College of Automation, Chongqing University, Chongqing, China

Abstract

Identifying the load and mutual inductance is essential for improving the power transfer capability and power transfer efficiency of Inductive Power Transfer (IPT) systems. In this paper, a steady-state load and mutual inductance identification method focusing on series-parallel compensated IPT systems is proposed. The identification model is established according to the steady-state characteristics of the system. Furthermore, two sets of identification results are obtained, and then they are analyzed in detail to eliminate the untrue one. In addition, the identification method can be achieved without extra circuits so that it does not increase the complexity of the system or the control difficulty. Finally, the feasibility of the proposed method has been verified by simulation and experimental results.

Key words: wireless power transfer, inductive power transfer, load identification, mutual inductance identification, resonant

I. INTRODUCTION

With the continuous development and progress of wireless power transfer (WPT) technologies, inductive power transfer (IPT) technology has attracted a lot of attention recently [1], [2]. Due to the advantages of low maintenance cost, high reliability, and flexible features, IPT systems have been widely applied in many occasions such as transportation [3]-[5], electronic products [6], [7], biomedical electronics [8], [9], and so on.

In IPT systems, the energy receiving side can be moved freely from the energy transmitting side, which leads to variations of the mutual inductance. In addition, different types of energy receiving equipment present different load characteristics. Taking the wireless power supplies for electric vehicles as an example, different electric vehicles have different power requirements and different mutual inductances on account of different heights and chassis alignments which may change the air gap between the transmitting coil and the receiving coil. Due to the inevitable variations mentioned above in practical IPT systems, the reflecting impedance from the receiving side to the transmitting side varies. Furthermore, the variation of the reflecting impedance results in a resonant frequency drifting, which dramatically reduces the power transfer capability and system efficiency [10]. Additionally, in order to ensure efficient and reliable power transfers, the output power of the system should be adjusted since the load change reflects the change in the actual power requirements. Therefore, load and mutual inductance identification is essential for IPT systems and is a key issue to improve the the transfer efficiency and the capability of IPT systems [11]-[15].

Previously, a few load identification methods have been researched [11]-[13], [15]. These methods achieve load identification when the mutual inductance is regarded as a constant parameter. Reference [14] achieves load and mutual inductance identification by switching an additional capacitor in the transmitting side. However, this method increases the complexity of the system and the control difficulty. Series-parallel compensated IPT systems have been discussed by a lot of scholars [16]-[18] and they have been applied in many fields such as biomedical implants [19] and battery charging [20] due to the current source characteristic of the parallel-compensated secondary side. However, existing load and mutual inductance identification methods mostly focus on series-series compensated IPT systems. Therefore, a

steady-state load and mutual inductance identification method for series-parallel compensated IPT systems is proposed in this paper. Only the information of the input voltage, the output current of the inverter and the system operating frequency are required in this method. Furthermore, this identification method can be achieved without any extra circuits. As a result, the cost and complexity of system is decreased.

II. FUNDAMENTAL ANALYSIS

A. Basic Circuit Topology

The topology of a series-parallel compensated IPT system as a commonly-used compensation scheme is shown in Fig. 1.

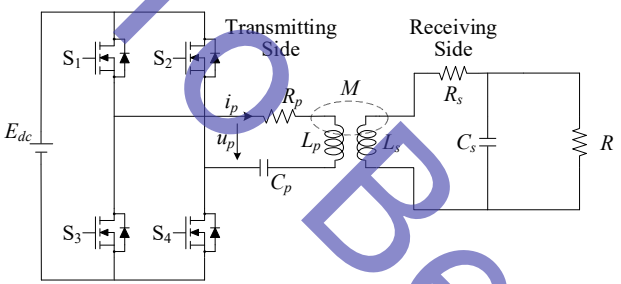

Fig. 1. Main circuit of a series-parallel compensated IPT system.

A typical IPT system consists of two independent mutually coupled coils in the transmitting and receiving side of the system. In this system, a DC voltage source E_{dc} supplies the power. A full-bridge inverter network is composed of four MOSFET switches, S_1, S_2, S_3 and S_4. The invert network generates a modulated ac voltage injected into the transmitting resonant network. A transmitting coil L_p in series with the compensating capacitor C_p constitutes a series resonant tank.

In the receiving side, the receiving coil L_s receives power from a high-frequency magnetic field and constitutes the parallel resonant network with the compensating capacitor C_s. Finally, the receiving side supplies power to the equivalent load R via the resonant network. R_p and R_s are the inherent resistances of L_p and L_s, respectively. M is the mutual inductance between the transmitting and receiving coils.

In order to achieve a maximum power transfer with a minimum VA rating of the supply, the system should operate at or near the inherent resonant frequency of the transmitting and receiving side. Thus, it is a logical choice to design the two inherent resonant frequencies at or near the same frequency ω_0, which satisfies the relationship:

$$\omega_0^2 \approx \frac{1}{L_p C_p} \approx \frac{1}{L_s C_s} \tag{1}$$

B. The equivalent circuit model

In the transmitting side, a combination of the coil and the compensating capacitance can be regarded as a low-pass filter, and the high frequency harmonic currents in the resonant network are supressed. Therefore, only the fundamental harmonic is considered for power transfer based on Fourier decomposition.

The output voltage of the full-bridge inverter is an approximately square wave with the amplitude of E_{dc}. Its fundamental harmonic u_p can be expressed as:

$$u_p(t) = \frac{4E_{dc}\sin\omega t}{\pi} \tag{2}$$

The root-mean-square (RMS) value of u_p is obtained by:

$$U_p = \frac{2\sqrt{2}E_{dc}}{\pi} \tag{3}$$

Therefore, the equivalent circuit model can be acquired, as illustrated in Fig. 2.

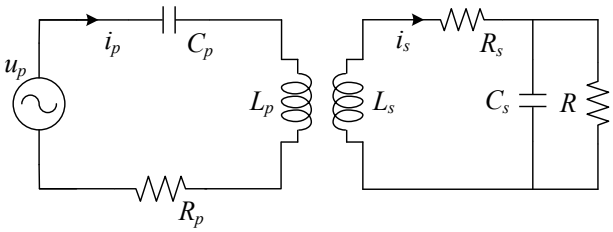

Fig. 2. Equivalent circuit model of a series-parallel compensated IPT system.

III. LOAD AND MUTUAL INDUCTANCE IDENTIFICATION

The output current i_p of the inverter can be expressed as:

$$i_p(t) = \sqrt{2}I_p\sin(\omega t + \varphi) \tag{4}$$

where, I_p is the RMS of i_p, and φ is the phase difference between u_p and i_p.

From Fig. 2, the KVL equation is derived as:

$$\begin{bmatrix} \dot{I}_p \\ \dot{I}_s \end{bmatrix} = \begin{bmatrix} Z_{11} & Z_{12} \\ Z_{21} & Z_{22} \end{bmatrix}^{-1} \cdot \begin{bmatrix} \dot{U}_p \\ 0 \end{bmatrix} \tag{5}$$

where

$$\begin{cases} Z_{11} = R_p + j\cdot\left(\omega L_p - \dfrac{1}{\omega C_p}\right) \\ Z_{12} = Z_{21} = j\omega M \\ Z_{22} = R_s + j\omega L_s + R \,\|\, \dfrac{1}{j\omega C_s} \end{cases} \tag{6}$$

Based on Eqn. (5), the expressions of $\dot{I}_p$ is conducted:

$$\dot{I}_p = \frac{\begin{vmatrix} \dot{U}_p & Z_{12} \\ 0 & Z_{22} \end{vmatrix}}{\begin{vmatrix} Z_{11} & Z_{12} \\ Z_{21} & Z_{22} \end{vmatrix}} \tag{7}$$

Then, the input impedance can be derived from Eqn. (7):

$$\frac{\dot{U}_p}{\dot{I}_p} = \alpha_1 + \frac{\alpha_2\gamma^2}{\alpha_2^2 + \beta_2^2} + j\left(\beta_1 - \frac{\beta_2\gamma^2}{\alpha_2^2 + \beta_2^2}\right) \tag{8}$$

where

$$\begin{cases} \alpha_1 = R_p \\ \alpha_2 = R_s + \dfrac{R}{1+\omega^2 C_s^{\,2} R^2} \\ \beta_1 = \omega L_p - \dfrac{1}{\omega C_p} \\ \beta_2 = \omega L_s - \dfrac{\omega C_s R^2}{1+\omega^2 C_s^{\,2} R^2} \\ \gamma = \omega M \end{cases} \tag{9}$$

Generally, in order to minimize the VA ratings of the power supply, it is desirable to make the system operate at the zero phase angle frequency. At this frequency, the input voltage u_p and input current i_p should be in phase, which means that φ is equal to zero and the following relationships can be obtained based on Eqn. (8).

$$\beta_1 - \frac{\beta_2 \gamma^2}{\alpha_2^{\,2} + \beta_2^{\,2}} = 0 \tag{10}$$

$$\frac{\dot{U}_p}{\dot{I}_p} = \frac{U_p}{I_p} = \alpha_1 + \frac{\alpha_2 \gamma^2}{\alpha_2^{\,2} + \beta_2^{\,2}} \tag{11}$$

Obviously, information on the equivalent load R is included in α_2 and β_2, while information on the mutual inductance M is included in γ. Consequently, two equations for the equivalent load R and the mutual inductance M, described in Eqns. (10) and (11), are obtained. Then, the identification results of the equivalent load R can be obtained by combining and solving the above equations.

$$R_1 = \frac{-1 - \sqrt{1 - 4c\left(R_s c + a - abc\right)\left(R_s - ab\right)}}{2c\left(R_s c + a - abc\right)} \tag{12}$$

$$R_2 = \frac{-1 + \sqrt{1 - 4c\left(R_s c + a - abc\right)\left(R_s - ab\right)}}{2c\left(R_s c + a - abc\right)} \tag{13}$$

Moreover, the coefficients are given as follows:

$$\begin{cases} a = \dfrac{U_p - \alpha_1 I_p}{\beta_1 I_p} \\ b = \omega L_s \\ c = \omega C_s \end{cases} \tag{14}$$

It is found that there are two solutions for R. Obviously, one of them is an untrue identification result while the other one is a reasonable solution. Therefore, in order to eliminate the untrue solution, a series of analysis is carried out.

To simplify the following analysing, a normalized angular frequency $\omega_n = \omega/\omega_0$ is defined, and the parameters β_1, α_2, β_2 and γ in Eqn. (9) are rewritten by substituting Eqn. (1).

$$\begin{cases} \alpha_2 = R_s + \dfrac{R}{1+\lambda^2 \omega_n^{\,2} R^2} \\ \beta_1 = \dfrac{\omega_n^{\,2} - 1}{\mu \omega_n} \\ \beta_2 = \dfrac{\omega_n + \lambda^2 \omega_n \left(\omega_n^{\,2} - 1\right) R^2}{\lambda\left(1+\lambda^2 \omega_n^{\,2} R^2\right)} \\ \gamma = \omega_n \omega_0 M \end{cases} \tag{15}$$

where

$$\begin{cases} \mu = \omega_0 C_p \approx \dfrac{1}{\omega_0 L_p} \\ \lambda = \omega_0 C_s \approx \dfrac{1}{\omega_0 L_s} \end{cases} \tag{16}$$

Based on Eqns. (15) and (16), the expressions of R_1 and R_2 can be rewritten as:

$$R_1 = \frac{1 + \sqrt{\Delta}}{2\lambda\omega_n\left(a\omega_n^{\,2} - \lambda\omega_n R_s - a\right)} \tag{17}$$

$$R_2 = \frac{1 - \sqrt{\Delta}}{2\lambda\omega_n\left(a\omega_n^{\,2} - \lambda\omega_n R_s - a\right)} \tag{18}$$

where

$$\Delta = 1 - 4\omega_n\left(a\omega_n^{\,2} - \lambda\omega_n R_s - a\right)\left(a\omega_n - \lambda R_s\right) \tag{19}$$

It should be noted that the rewritten expressions of R_1 and R_2 are based on Eqn. (16) as mentioned before. However, $\omega_0 C_p$ and $\omega_0 C_s$ are approximately equal to $1/\omega_0 L_p$ and $1/\omega_0 C_s$ in actual systems. Therefore, the identification results of the equivalent load R shown in Eqns. (12) and (13) are more accurate. The expressions of R_1 and R_2 shown in Eqns. (17) and (18) are only used for the subsequent analysis.

According to Eqns. (17) and (18), it is found that the value of the equivalent load R is correlated with ω_n. Therefore, in order to obtain the actual identification result of the equivalent load, the ranges of R_1 and R_2 are discussed in three cases, namely $\omega_n<1$, $\omega_n=1$, and $\omega_n>1$.

A. $\omega_n<1$

In this case, it is found that the value of R_1 is positive, while the value of R_2 is negative, which are depicted in Fig. 3 and Fig. 4, respectively. In addition, K represents the ratio between U_p and I_p. Obviously, R_1 is the identification result of the equivalent load R.

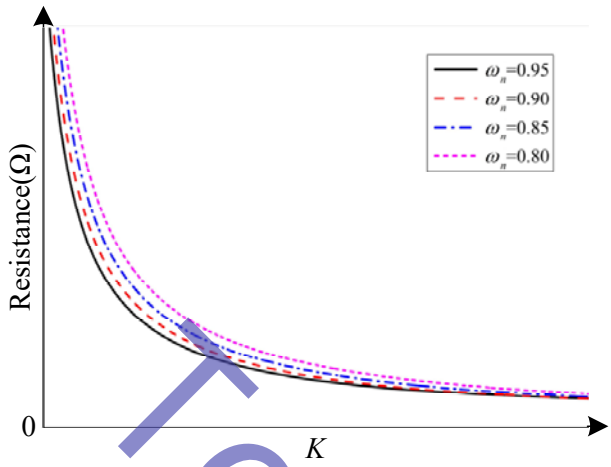

Fig. 3. Range of R_1 versus K at different values of ω_n when ω_n<1.

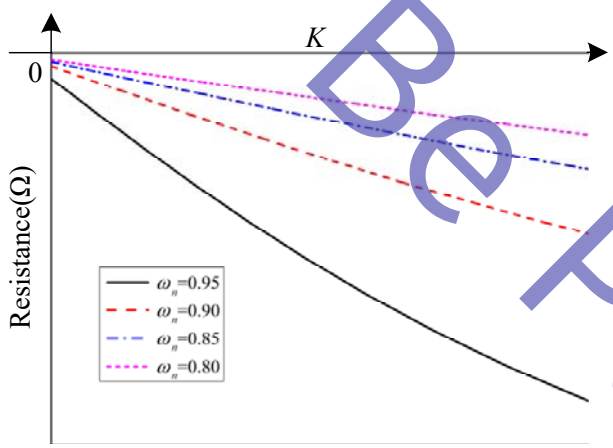

Fig. 4. Range of R_2 versus K at different values of ω_n when ω_n<1.

B. ω_n=1

When ω_n=1, the following equation can be achieved by the transformation of Eqn. (10).

$$\frac{\beta_2}{\alpha_2^{\,2}+\beta_2^{\,2}}\cdot\omega_0^{\,2}M^2=0 \tag{20}$$

where

$$\begin{cases}\alpha_2=R_s+\dfrac{\mathrm{R}}{1+\lambda^2R^2}\\ \beta_2=\dfrac{1}{\lambda\left(1+\lambda^2R^2\right)}\end{cases} \tag{21}$$

Obviously, β_2 is greater than 0. Therefore, Eqn. (20) is valid only when M=0. This means that the energy receiving part is completely removed.

C. ω_n>1

The coupling coefficient k of the system is defined as:

$$k=\frac{M}{\sqrt{L_pL_s}}\Rightarrow M=k\sqrt{L_pL_s} \tag{22}$$

Eqn. (22) is substituted into Eqn. (10) to obtain the expression of k below.

$$k=\frac{1}{\omega_n}\sqrt{\frac{\mu\lambda\beta_1\left(\alpha_2^{\,2}+\beta_2^{\,2}\right)}{\beta_2}} \tag{23}$$

Making

$$\frac{\mathrm{d}}{\mathrm{d}R}k=0 \tag{24}$$

Then, the value of R_0 corresponding to the maximum coupling coefficient can be obtained as:

$$R_0=\frac{R_s}{\omega_n^{\,2}-1} \tag{25}$$

The coupling coefficient k is monotonically increasing when the load R is in the range of (0, R_0), and it decreases with a monotonically increasing R when R is larger than R_0. Therefore, the maximum value and the minimum value of k can be expressed as follows:

$$\begin{cases}k_{\max}=k\big|_{R=R_0}=\sqrt{\dfrac{\omega_n^{\,2}+\lambda^2R_s^{\,2}-1}{\omega_n^{\,2}}}\\ k_{\min}=k\big|_{R\to+\infty}=\sqrt{\dfrac{\omega_n^{\,4}+\left(\lambda^2R_s^{\,2}-2\right)\omega_n^{\,2}+1}{\omega_n^{\,4}}}\end{cases} \tag{26}$$

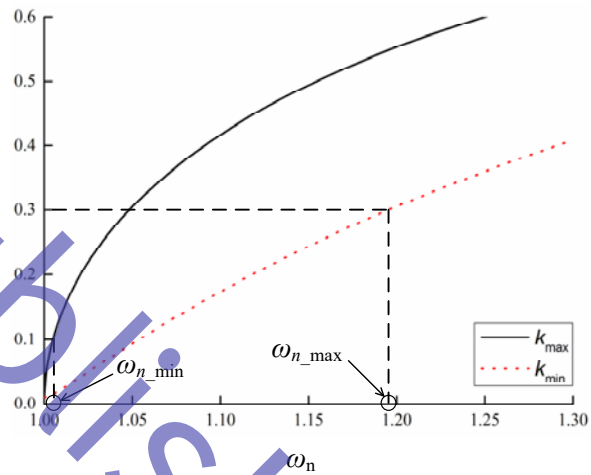

Fig. 5. Variation of k_{max} and k_{min} for different values of ω_n.

Based on Eqn. (26), the curves of k_{max} and k_{min} for various values of ω_n can be plotted as shown in Fig. 5. Typically, the coupling coefficient k is in the range of 0.1–0.3 [21]. Under this condition, the range of the normalized angular frequency ω_n can be calculated according to Fig. 5.

$$\begin{aligned}&\left\{\omega_n>1\right\}\cap\left\{\sqrt{\frac{\omega_n^{\,2}+\lambda^2R_s^{\,2}-1}{\omega_n^{\,2}}}\ge0.1\right\}\\ &\cap\left\{\sqrt{\frac{\omega_n^{\,4}+\left(\lambda^2R_s^{\,2}-2\right)\omega_n^{\,2}+1}{\omega_n^{\,4}}}\le0.3\right\}\\ &\Rightarrow1.005\le\omega_n\le1.195\end{aligned} \tag{27}$$

Consequently, the range of the load identification results can be obtained when ω_n satisfies the relationship given in Eqn. (27), which is illustrated in Fig. 6. It can be seen that: 1) both R_1 and R_2 are positive; 2) R_1 is larger than R_{uni} and R_2 is less

than R_{uni}. From Eqns. (17) and (18), a unique solution R_{uni} exists when Δ is equal to zero. In addition, in this case, R_1 and R_2 are equal to R_{uni}.

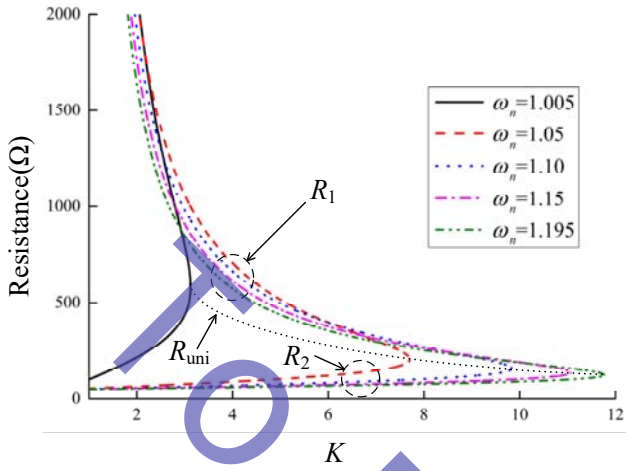

Fig. 6. Ranges of R_1 and R_2 versus K at different values of ω_n when ω_n>1.

A plot of R_{uni} at various normalized angular frequencies is shown in Fig. 7. It can be seen that R_{uni} decreases with an increasing ω_n. The minimum value of R_{uni} is larger than 100Ω. In most applications, such as battery charging systems, the equivalent resistance is typically just a few tens of ohms [20], [22]. Therefore, R_2 is considered as an identification result of equivalent load.

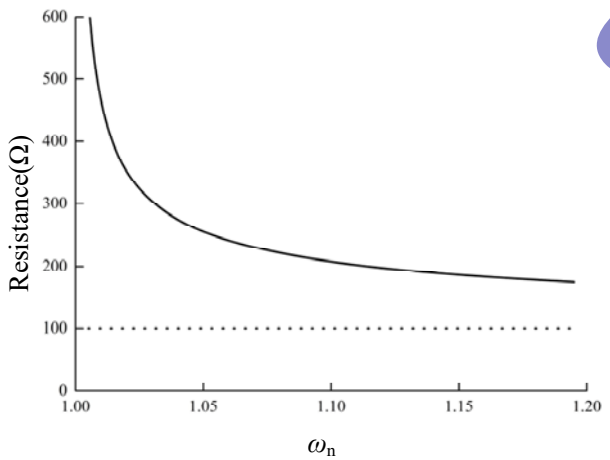

Fig. 7. Variation of R_{uni} for various values of ω_n.

In conclusion, the identification result of the equivalent load R can be expressed as follows:

$$R=\begin{cases} R_1 & \omega_n<1 \\ \text{None} & \omega_n=1 \\ R_2 & \omega_n>1 \end{cases} \tag{28}$$

The expressions of R_1 and R_2 are given in Eqns. (12) and (13). Furthermore, the identification results of the mutual inductance M can be obtained based on Eqn. (10).

$$M=\begin{cases} \dfrac{1}{\omega}\sqrt{\dfrac{\beta_1\left(\alpha_2^2+\beta_2^2\right)}{\beta_2}} & \omega_n\neq 1 \\ 0 & \omega_n=1 \end{cases} \tag{29}$$

According to Eqns. (28) and (29), the identification results are calculated based on the circuit parameters (namely L_p, L_s, C_p, C_s, R_p, R_s). This means that the results are influenced by variations of these parameters. In general, under normal circuit operating conditions, the circuit parameters do not change much. Therefore, these parameters are generally assumed to be constant [11]-[15]. Then, the identification results can be obtained by detecting the input voltage E_{dc}, the output current I_p of the inverter and the system operating frequency f when the system is in operation.

IV. Simulation and Experimental Studies

A. Parameters and Structure of the Proposal

In order to verify the effectiveness of the proposed method, a simulation model based on MATLAB/Simulink is set up with reference to Fig. 1. The main parameters are the same in both the simulation and experimental systems, and they are listed in Table I.

TABLE I
Main Parameters of the Series-Parallel Compensated IPT System

Parameters	Values
Transmitting coil L_p (μH)	152.87
Receiving coil L_s (μH)	153.60
Compensation capacitance C_p (nF)	68.26
Compensation capacitance C_s (nF)	67.73
Inherent resistance of transmitting coil R_p (Ω)	0.49
Inherent resistance of receiving coil R_s (Ω)	0.54

A structure diagram of the proposed identification method is shown in Fig. 8. The zero phase angle condition is achieved by the frequency adjustment based on the phase detection of the output current and voltage of the inverter. The values of E_{dc}, I_p and f are measured by the detection unit including the DC voltage measurement, the current RMS sampling and the operating frequency detection, respectively. Then, the measured data are transferred to the identification unit and the values of the load resistance and the mutual inductance are calculated by the algorithm depicted in Section III.

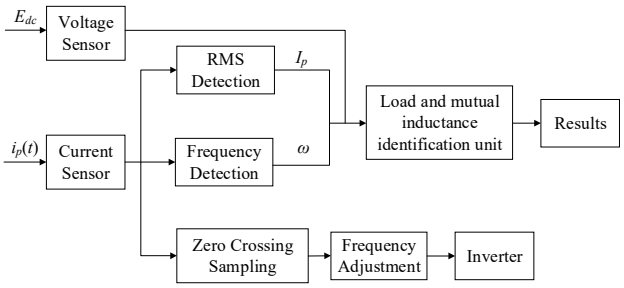

Fig. 8. Structure of the proposed identification method.

B. *Simulation Results*

The total simulation time is set at 0.2ms and the system has already reached the steady-state. The maximum simulation step is 0.1μs.

The identification accuracy of the load resistance R and the mutual inductance M are presented in Fig. 9 and Fig. 10, when the mutual inductance varies from 15μH to 45μH and the load resistance variation ranges from 10Ω to 50Ω. It can be seen that the identification accuracy of R and M are more than 96% and 97%, when the mutual inductance M is 15μH. Moreover, the identification accuracies of R and M increase to about 98% and 98.5%, when the mutual inductance increases to 20μH. The identification accuracy is slightly lower when the mutual inductance is too small.

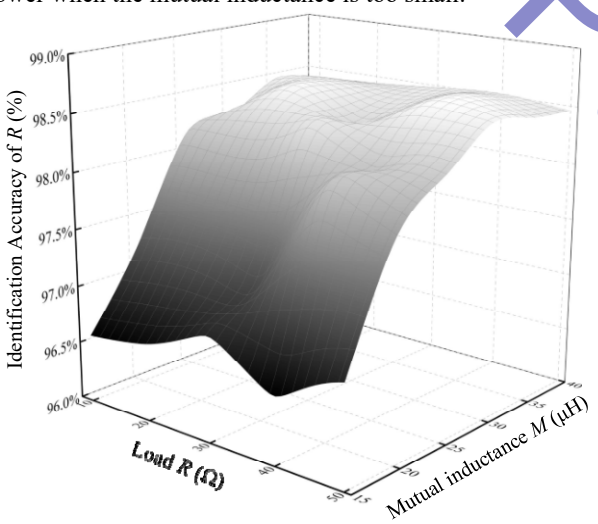

Fig. 9. Simulated identification accuracy of the load resistance R.

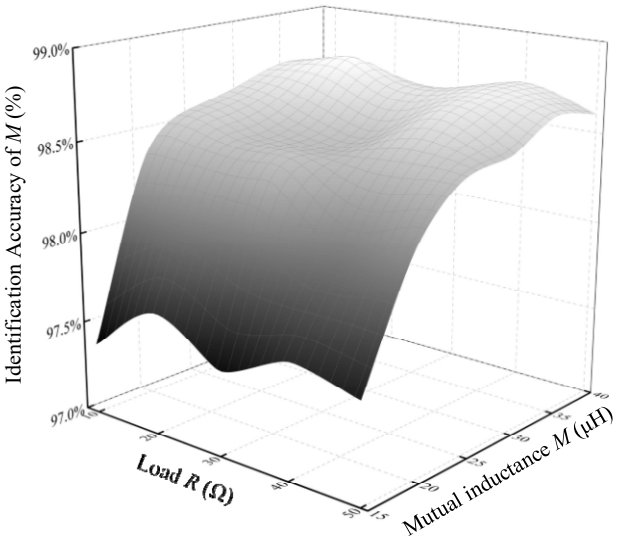

Fig. 10. Simulated identification accuracy of the mutual inductance M.

Furthermore, the simulated values of ω_n are illustrated in Fig. 11. It can be seen that ω_n increases slightly with a growing M and that the variation of R has little effect on ω_n. When M and R are set at 15μH and 50Ω, the minimum value of ω_n ($\omega_n \approx 1.0051$) is achieved. In addition, through simulations, it is found that ω_n is less than 1 when the coupling coefficient is very low ($k<0.01$). For example, the simulated values of the load resistance and the mutual inductance are set at 20Ω and 1μH ($\omega_n<1$). In addition, the identification results are 18.46Ω and 1.17μH with accuracies of 92.3% and 83%, respectively. However, as mentioned above, the coupling coefficient k typically ranges from 0.1 to 0.3 (i.e. the mutual inductance of this system ranges from approximately 15μH to 46μH). It can be considered that $\omega_n>1$ is the most ordinary operating condition of IPT systems. Therefore, the simulations and the experiments in this paper are focusing on the case of $\omega_n>1$.

Altogether, the simulation results verify that the proposed identification model is effective for identifying the load resistance and the mutual inductance.

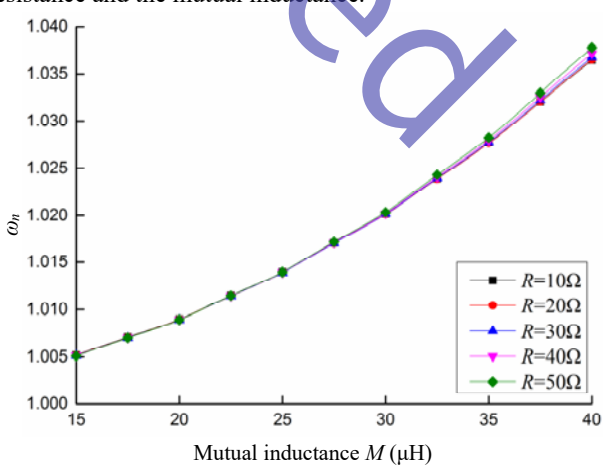

Fig. 11. Simulated values of ω_n at different values of R and M.

C. Experimental Results

A prototype of the series-parallel compensated IPT system, as shown in Fig. 12, was built and practically tested. The full-bridge inverter circuit is made up of four MOSFETs (STP30NF20). A FPGA chip (Altera Cyclone II EP2C5T144C8) is selected as a controller of the system, which calculates the values of the load resistance and the mutual inductance.

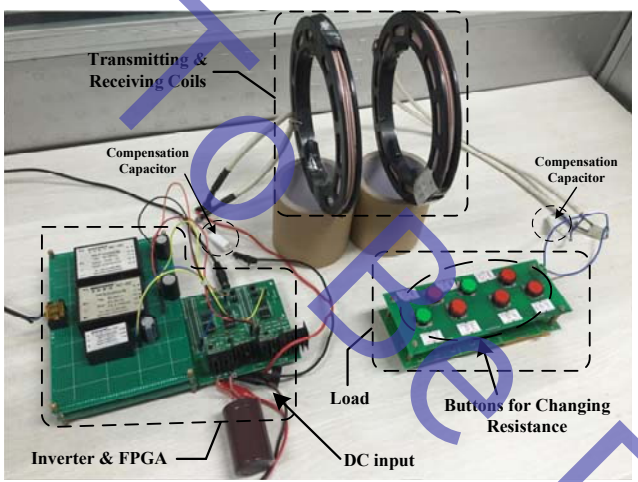

Fig. 12. Experimental setup.

Table II shows the identification results of R and M when the load resistance is fixed at 30Ω and the mutual inductance varies from 15μH to 45μH. Actually, the mutual inductances are 15.06μH, 20.48μH, 25.66μH, 30.51μH, 35.63μH and 40.08μH, and they are changed by adjusting the relative position between the transmitting coil and the receiving coil.

It is found that identification accuracy grows according to increases in the mutual inductance. The accuracy drops to the lowest value when the mutual inductance is set to 15.06μH, which agrees well with the simulation results. The maximum identification error of R is 4.27%, and the maximum identification error of M is 3.65%.

TABLE II
IDENTIFICATION EXPERIMENTAL RESULTS WHEN THE LOAD RESISTANCE R IS FIXED

R	M	Identified R	Identified M
30Ω	15.06μH	31.28Ω	15.61μH
30Ω	20.48μH	28.94Ω	20.98μH
30Ω	25.66μH	30.89Ω	26.22μH
30Ω	30.51μH	30.77Ω	29.82μH
30Ω	35.63μH	29.01Ω	36.47μH
30Ω	40.08μH	30.71Ω	40.98μH

Similarly, experiments with a fixed mutual inductance of 30.51μH and load resistances changing from 10Ω to 50Ω have been performed. The load resistance is regulated by pressing the buttons shown in Fig 12. The identification results of R and M are illustrated in Table III. The maximum identification error of R is 5.50%, and the maximum identification error of M is 4.42%.

TABLE III
IDENTIFICATION EXPERIMENTAL RESULTS WHEN THE MUTUAL INDUCTANCE M IS FIXED

R	M	Identified R	Identified M
10Ω	30.51μH	9.45Ω	31.86μH
20Ω	30.51μH	20.76Ω	31.39μH
30Ω	30.51μH	30.77Ω	29.82μH
40Ω	30.51μH	38.75Ω	29.84μH
50Ω	30.51μH	51.52Ω	31.16μH

In addition, more experiments were performed when the mutual inductance was in the range of 15μH–46μH. According to the obtained results, the identification accuracies of R and M can both be maintained over 90% when the load resistance ranges from 8Ω to 95Ω. The ranges of R and M can be expanded by sacrificing the identification accuracy. The feasibility of the proposed identification method has been verified with different loads and varying mutual inductances.

V. CONCLUSION

In this paper, a load and mutual inductance identification method for series-parallel compensated IPT systems is proposed. Only information on the input voltage, the output current of inverter and the system operating frequency are required in this method. The simulation results and the set values were in close agreement. Experimental results showed that the identification accuracy is over 90% when the load resistance varies from 8Ω to 95Ω, and that the mutual inductance is in the range of 15μH–46μH. Both the simulation and experimental results have verified the feasibility of the proposed method. Although only the series-parallel compensation scheme is discussed in this paper, the proposed method has some reference value for other types of secondary parallel-compensated IPT systems. Moreover, the influence of some of the intrinsic factors, such as variation of the circuit parameters, on the identification results will be considered in future research.

ACKNOWLEDGEMENT

This work was sponsored by the research funds for the National Natural Science Foundation of China under Grants #51477020 and #61573074. This work was also supported by Chongqing International Science and Technology Cooperation Base Project under Grants CSTC2015GJHZ40001.

REFERENCES

[1] G. A. Covic and J. T. Boys, "Inductive Power Transfer," *Proceedings of the IEEE*, Vol. 101, pp. 1276-1289, Jun.

2013.
[2] R. Mai, Y. Li, L. Lu, and Z. He, "A Power Regulation and Harmonic Current Elimination Approach for Parallel Multi-Inverter Supplying IPT Systems," *Journal of Power Electronics*, Vol. 16, No.4, pp. 1245-1255, Jul. 2016.
[3] C. Ma, S. Ge, Y. Guo, L. Sun, and C. Liu, "Investigation of a SP/S Resonant Compensation Network Based IPT System with Optimized Circular Pads for Electric Vehicles," *Journal of Power Electronics*, Vol. 16, No.6, pp. 2359-2367, Nov. 2016.
[4] S. Li, and C. C. Mi, "Wireless Power Transfer for Electric Vehicle Applications," *IEEE Journal of Emerging and Selected Topics in Power Electronics*, Vol. 3, No. 1, pp. 4-17, Mar. 2015.
[5] H. Z. Z. Beh, G. A. Covic and J. T. Boys, "Investigation of Magnetic Couplers in Bicycle Kickstands for Wireless Charging of Electric Bicycles," *IEEE Journal of Emerging and Selected Topics in Power Electronics*, Vol. 3, No. 1, pp. 87-100, May. 2015.
[6] S. Y. Hui, "Planar Wireless Charging Technology for Portable Electronic Products and Qi," *Proceedings of the IEEE*, Vol. 101, No. 6, pp. 1290-1301, Mar. 2013.
[7] Y. Jang, and M. M. Jovanovic, "A contactless electrical energy transmission system for portable-telephone battery chargers," *IEEE Transactions on Industrial Electronics*, Vol. 50, No. 3, pp. 520-527, Jun. 2003.
[8] A. P. Hu, Y. W. You, F. B. Chen, D. McCormick, D. M. Budgett, "Wireless Power Supply for ICP Devices With Hybrid Supercapacitor and Battery Storage," *IEEE Journal of Emerging and Selected Topics in Power Electronics*, Vol. 4, No. 1, pp. 273-279, Mar. 2016.
[9] D. Ahn and S. Hong, "Wireless Power Transmission with Self-Regulated Output Voltage for Biomedical Implant," *IEEE Transactions on Industrial Electronics*, Vol. 61, No. 5, pp. 2225-2235, Jul. 2014.
[10] D. Seo, J. Lee and H. Lee, "Optimal Coupling to Achieve Maximum Output Power in a WPT System," *IEEE Transactions on Power Electronics*, Vol. 31, No. 6, pp. 3994-3998, Jun. 2016.
[11] Z. Wang, Y. Li, Y. Sun, C. Tang, and X. Lv, "Load Detection Model of Voltage-Fed Inductive Power Transfer System,", *IEEE Transactions on Power Electronics*, Vol. 28, No. 11, pp. 5233-5243, Feb. 2013.
[12] J. Yin, D. Lin, C. Lee, and S. Y. R. Hui, "A Systematic Approach for Load Monitoring and Power Control in Wireless Power Transfer Systems Without Any Direct Output Measurement," *IEEE Transactions on Power Electronics*, Vol. 30, No. 3, pp. 1657-1667, Apr. 2015.
[13] Y. Su, L. Chen, Z. Wang, A. P. Hu and X. Dai, "A Load Identification Method for Inductive Power Transfer System Based on the Least Squares Algorithm," *Transactions of China Electrotechnical Society*, Vol. 30, No. 5, pp. 9-14, Mar. 2015.
[14] J. Yin, D. Lin, C. K. Lee, T. Parisini, and S. Y. R. Hui, "Front-End Monitoring of Multiple Loads in Wireless Power Transfer Systems Without Wireless Communication Systems," *IEEE Transactions on Power Electronics*, Vol. 31, No. 3, pp. 2510-2517, Apr. 2016.
[15] Y. Su, H. Zhang, Z. Wang, A. P. Hu, L. Chen, and Y. Sun, "Steady-State Load Identification Method of Inductive Power Transfer System Based on Switching Capacitors," *IEEE Transactions on Power Electronics*, Vol. 30, No. 5, pp. 9-14, Mar. 2015.
[16] S. Guo, and H. Lee, "An Efficiency-Enhanced CMOS Rectifier With Unbalanced-Biased Comparators for Transcutaneous-Powered High-Current Implants," *IEEE Journal of Solid-State Circuits*, Vol. 44, No. 6, pp. 1796-1804, Jun. 2009.
[17] J. Sallan, J. L. Villa, A. Llombart and J. F. Sanz, "Optimal Design of ICPT Systems Applied to Electric Vehicle Battery Charge," *IEEE Transactions on Industrial Electronics*, Vol. 56, No. 6, pp. 2140-2149, Jun. 2009.
[18] Y. Liu, A. P. Hu and U. K. Madawala, "Maximum Power Transfer and Efficiency Analysis of Different Inductive Power Transfer Tuning Topologies," *2015 IEEE 10th Conference in Industrial Electronics and Applications (ICIEA),* pp. 649-654， 2015.
[19] Z. Pantic. and S. M. Lukic, "Framework and Topology for Active Tuning of Parallel Compensated Receivers in Power Transfer Systems," *IEEE Transactions on Power Electronics,* Vol. 27, No. 20, pp. 4503-4513, Nov. 2012.
[20] W. Zhang, S. Wong, C. K. Tse, and Q. Chen, "Load-Independent Duality of Current and Voltage Outputs of a Series- or Parallel-Compensated Inductive Power Transfer Converter With Optimized Efficiency," *IEEE Journal of Emerging and Selected Topics in Power Electronics*, Vol. 3, No. 1, pp. 137-146, Mar. 2015.
[21] M. J. Neath, A. K. Swain, U. K. Madawala, and D. J. Thrimawithana, "An optimal PID controller for a bidirectional inductive power transfer system using multiobjective genetic algorithm," *IEEE Transactions on Power Electronics*, Vol. 29, No. 3, pp. 1523-1531, Mar. 2014.
[22] X. Qu, H. Han, S. Wong, C. K. Tse, and W. Chen, "Hybrid IPT Topologies With Constant Current or Constant Voltage Output for Battery Charging Applications," *IEEE Transactions on Power Electronics*, Vol. 30, No. 11, pp. 6329-6337, Nov. 2015.

Long Chen received his B.S. degree in Medical Information from Southern Medical University, Guangzhou, China, in 2011. He is presently working towards his Ph.D. degree in Control Theory and Control Engineering from the College of Automation, Chongqing University, Chongqing, China. His current research interests include the load identification and optimization of wireless power transfer systems.

Yu-Gang Su received his B.S. and M.S. degrees in Industry Automation, and his Ph.D. degree in Control Theory and Control Engineering from Chongqing University, Chongqing, China, in 1985, 1993 and 2004, respectively. From 2008 to 2009, he was a Visiting Scholar at the University of Queensland, Brisbane, QLD, Australia. He is presently working as a Professor in the College of Automation, Chongqing University. His current research interests include power electronics, control theory and applications, and wireless power transfer.

Yu-Ming Zhao received his B.S. degree from the College of Automation of Chongqing University, Chongqing, China, in 2014, where he is presently working towards his Ph.D. degree in Control Theory and Control Engineering in the College of Automation. His current research interests

include capacitively coupled power transfer and its modelling.

Chun-Sen Tang (S'08–M'09) received his B.S. and Ph.D. degrees from the College of Automation, Chongqing University, Chongqing, China, in 2004 and 2009, respectively. In 2008, he was a Research Fellow in the Department of Electrical and Computer Engineering, University of Auckland, Auckland, New Zealand. He joined the College of Automation, Chongqing University, in 2009, where he is presently working as an Associate Professor. His current research interests include nonlinear modeling and analysis, intelligent control, and wireless power transfer.

Xin Dai received the B.S. degree in Industrial Automation from Yuzhou University, Chongqing, China, in 2000; and his Ph.D. degree in Control Theory and Control Engineering from the School of Automation, Chongqing University, Chongqing, China, in 2006. In 2012, he was a Visiting Scholar at the University of Auckland, Auckland, New Zealand. He is presently working as a Professor in the School of Automation, Chongqing University. His current research interests include inductive power transfer technology and nonlinear dynamic behavior analysis of power electronics.